Tellus (2002), 54A, 245–259
Printed in UK. All rights reserved

TELLUS
ISSN 0280–6495

Sea ice concentration anomalies as long range predictors of anomalous conditions in the North Atlantic basin

By E. SÁNCHEZGÓMEZ, W. CABOSNARVAÉZ and M. J. ORTIZBEVIÁ, *Departamento de Física, Facultad de Ciencias, Universidad de Alcalá, Alcalá de Henares, Madrid 28871, Spain*

(Manuscript received 23 May 2001; in final form 6 December 2001)

ABSTRACT

Long-range empirical forecasts of North Atlantic anomalous conditions are issued, using sea ice concentration anomalies in the same region as predictors. Conditions in the North Atlantic are characterized by anomalies of sea surface temperature, of 850 hPa air temperature and of sea level pressure. Using the Singular Value Decomposition of the cross-covariance matrix between the sea ice field (the predictor) and each of the predictand variables, empirical models are built, and forecasts at lead times from 3 to 18 months are presented. The forecasts of the air temperature anomalies score the highest levels of the skill, while forecasts of the sea level pressure anomalies are the less sucessful ones.

To investigate the sources of the forecast skill, we analyze their spatial patterns. In addition, we investigate the influence of major climatic signals on the forecast skill. In the case of the air temperature anomalies, the spatial pattern of the skill may be connected to El Niño Southern Oscillation (ENSO) influences. The ENSO signature is present in the predictor field, as shown in the composite analysis. The composite pattern indicates a higher (lower) sea ice concentration in the Labrador Sea and the opposite situation in the Greenland–Barents Seas during the warm (cold) phase of ENSO. The forecasts issued under the El Niño conditions show improved skill in the Labrador region, the Iberian Peninsula and south of Greenland for the lead times considered in this paper. For the Great Lakes region the skill increases when the predictor is under the influence of a cold phase. Some features in the spatial structure of the skill of the forecasts issued in the period of the Great Salinity Anomaly present similarities with those found for forecasts made during the cold phase of ENSO. The strength of the dependence on the Great Salinity Anomaly makes it very difficult to determine the influence of the North Atlantic Oscillation.

1. Introduction

Atmospheric conditions at midlatitudes typically change during one week, whereas in the ocean, conditions persist longer. For this reason, climatologists turn to the ocean to issue long-term forecasts of atmospheric variability. In a first aproximation, the anomalous variability of midlatitude oceans can be modelled as a linear response to the stochastic atmospheric forcing (Frankignoul and Hasselmann, 1977). This red noise variability, associated with the larger spatial and longer temporal scales, could in turn feed back on the atmosphere in ways yet to be explored (Deser et al., 2000). The interannual variability of sea ice, forced by the atmospheric circulation, through wind stress and heat fluxes (Walsh and Johnson, 1979; Fang and Wallace, 1994), can also be explained as the local response to atmospheric forcing (Lemke et al., 1980). Thereafter the sea ice pattern might force some atmospheric variability (Mysak and Venegas, 1998). On the other hand, it has been shown that sea ice concentration

* Corresponding author.

(hereinafter SIC) anomalies present a moderate ENSO influence (Gloersen, 1995; Mysak et al., 1996).

The bases for long-range forecasting in the North Atlantic were laid by Radcliffe and Murray (1970), who pointed at the lagged correspondence between North Atlantic sea surface temperature (hereafter SST) anomalies and European pressure field. There are a number of empirical models that explore the skill of SST anomalies at predicting the North Atlantic atmospheric variability (Barnett et al., 1984; Johansson et al., 1998; Vautard et al., 1998). The authors of the present work have also tackled this topic in a previous paper (SánchezGómez et al., 2001). In it, the same statistical technique (singular value decomposition, SVD, of the cross-covariance matrix) and the same forecast scheme, were employed to forecast 850 hPa air temperature (T850) anomalies in the North Atlantic, taking SST anomalies as well as various atmospheric variables as predictors. The assessment of the skill of the sea ice concentration anomalies at forecasting the atmospheric circulation in the North Atlantic basin is a natural extension of this previous work.

Figure 1 is a reproduction of Fig. 10 in Deser and Blackmon (1993). It shows the lagged correlation between the standardized time series of the second empirical orthogonal function (EOF) of the North Atlantic winter SST and the SIC anomalies averaged over the Davis Strait–Labrador Sea region. This relationship suggests that the SIC anomalies could be used to forecast the evolution of SST anomalies about 1 or 2 years in advance. The second EOF of winter SST (not shown) explains a 24% of the total variance of the field and is a tripole pattern with one center of action in eastern Newfoundland covarying out-of-phase with two centers situated one over the northeastern Atlantic and northern Europe, and the other over Bermuda and the Caribbean Sea and Gulf Stream region. The first EOF, which accounts for 26% of the variance, is scarcely related to SIC.

SIC anomalies in the Labrador sea could influence, in a few months, the waters near Bermuda through advection by the Labrador current and further entrainment by the Gulf Stream (Pickart et al., 1997). SIC anomalies could also reach this region through subsurface transport, and in this way, their influence could be noticed after more than one year (Curry et al., 1998). However, due to the regional nature of sea ice, it is not clear whether SIC anomalies could predict the large-scale conditions in the North Atlantic. Our aim is to test this possibility with an empirical forecast model. We then investigate the origin of the forecast skill, which leads to a better knowledge of the atmospheric and oceanic variability in the North Atlantic basin.

The paper is organized as follows: in Section 2 we describe the data used as predictor and predictand fields as well as the details of their preliminary treatment. An analysis of the fields involved in the forecasts is briefly presented in Section 3. Section 4 contains a short description of the forecast scheme and in Section 5 the results are

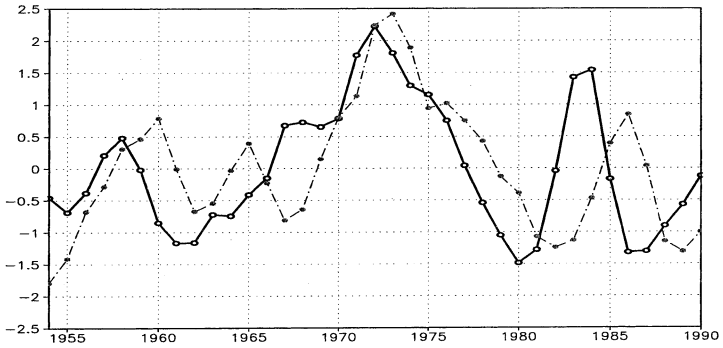

Fig. 1. Reproduction of Fig. 10 in Deser and Blackmon (1993): time series of the second EOF of winter (November–March) SST anomalies (dashed) and SIC anomalies averaged in the Davis Strait–Labrador Sea region (solid). The second EOF of winter SST anomalies explains a 24% of the variance. Both time series have been standardized and detrended.

presented and analyzed. Finally the findings are summarized and discussed in Section 6.

2. Data

Two atmospheric variables are used here to characterize the anomalous atmospheric circulation: 850 hPa air temperature (T850) and sea level pressure (SLP) anomalies. T850 has the advantage of being closely connected to sea level air temperature, while not being sensitive to the different topographies of the GCM models, and it is known to be well represented in the NCEP Reanalyses (T. Palmer, personal communication, 1997). Sea level pressure is directly related to the global atmospheric circulation, and it is by far the longest and best observational dataset available.

Data of T850 for the period 1958–1998 are extracted from the NCEP Reanalyses dataset (Kalnay et al., 1996; http://www.cdc.noaa.gov/), and anomalies computed by subtraction of this 41-year climatology. The resultant field contains monthly anomalies, in a $2.5^\circ \times 2.5^\circ$ grid. The SLP data were obtained from the GMSLP dataset from the Hadley Centre, and are monthly means given in a $5^\circ \times 5^\circ$ grid. The period 1950–1994 nearly coincides with that of the air temperature above and is selected from the available record length (1881–1994) and its climatology removed in order to obtain SLP anomalies. SST data are part of the HadISST1 dataset (Rayner et al., 2000), also from the Hadley Centre. For the reasons explained above, we work with the last 50 years, then anomalies are obtained from the 1950–1999 climatology. Originally on a $1^\circ \times 1^\circ$ grid, thses data have been interpolated to a $2^\circ \times 2^\circ$ grid.

The common domain of the three predictand fields (SLP, SST and T850 anomalies) is the North Atlantic basin, from 90°W to 10°E, and from 20°N to 90°N as can be appreciated in Fig. 6, for instance. In the east, the region selected includes large part of coastal Europe. In the west, it includes part of the US and Canadian coast, and also the Caribbean, a region of tropical–extratropical interactions.

As predictor field, we have used SIC anomalies in the Greenland Sea, Labrador Sea and Davis Strait. They were obtained from the HadISST record (Hadley Centre) from 1871 to 1998, and range from 0 (no sea ice) to 1 (maximum sea ice concentration). They are monthly data, gridded $1^\circ \times 1^\circ$. Because of the paucity of the data before 1950, we have decided to start the analysis only after January 1950. SIC anomalies are obtained in the same way as for the other fields.

Since we are interested in long-range forecasts, a preliminary filtering has been used to focus on the variability associated with the large spatial and longer temporal scales. The atmospheric spectrum shows a significant peak at the period around 7–8 months and much noise below 6 months. The SIC anomalies spectrum is essentially red, with a strong annual and semi-annual dependency (the latter absent in the atmospheric spectra). To optimize the performance of the SVD method, and prior to each forecast realization, we filter the time series of predictor and predictand fields, removing the variability in timescales shorter than 8 months. This filter is computed in the time domain, using the convolution form. Let r_l be the smoothing function and s_k the time series to be filtered, then the discrete convolution of these functions is:

$$s'_j = (r * s)_j = \sum_{k=-(L/2)+g(j)}^{(L/2)+h(j)} s_{j+k} r_{j+k} \qquad (1)$$

$$h(j) = 0, \quad g(j) = \frac{L}{2} - + 1; \quad 1 \leqslant j \leqslant \frac{L}{2}$$

$$h(j) = g(j) = 0; \quad \frac{L}{2} + 1 \leqslant j \leqslant N - \frac{L}{2}$$

$$h(j) = -\frac{L}{2} + N - j, \quad g(j) = 0;$$

$$N - \frac{L}{2} + 1 \leqslant j \leqslant N$$

where $j = 1, \ldots, N$, L is the width of the smoothing function, and h, non-zero only near the borders, allows the window to become asymmetric there, thereby avoiding the inclusion of any information of the future into the training sample. In this way we ensure that the prediction issued is a real forecast. Predictor and predictand fields are split into training sample and validation period. The training sample includes those points used to compute the cross-covariance matrix. The validation period is formed by the forecast months. The same convolution filter is used through all the forecasts, and through all the experiments.

To study the origin of the skill we take into account three major climatic signals: the Great

Salinity Anomaly, the El Niño Southern Oscillation (ENSO) and the North Atlantic Oscillation (NAO). The latter two signals are respectively monitored by their indices: the Niño3 index [averaged SST anomalies in the Niño3 region (150°W–90°W, 5°S–5°N)] and the NAO index, calculated from the filtered (periods shorter than 8 months were removed) SLP anomalies data as the difference between Lisbon (Portugal) and Stykkisholmur (Iceland), according to Hurrell (1996).

3. Analysis of predictor and predictand data sets

A preliminary analysis of the distinct fields in terms of their respective EOFs has been performed. In this way, we try to determine the spatial scales favoured for each variable. The EOFs temporal coefficients, or principal components (PCs), allowed us to identify preferred timescales of variability. The first EOF of the predictor field (SIC anomalies), represented in Fig. 2, shows the highest loadings over the Greenland Sea. This spatial pattern, which explains 66% of the variance of original field, as well as its evolution in time (Fig. 3a), resembles the first EOF of Deser et al. (2000). All seasons, not only winter as in the mentioned work, have been used in our analysis, which could explain the absence here of the out-of-phase relationship between the Greenland-Barents and Labrador Seas. Nevertheless there is a bimodal character in the pattern of Fig. 2, as reflected in the different magnitudes of the loadings in Labrador and Greenland-Barents Seas. The time coefficient in Fig. 3a also shows a difference in the behaviour of SIC anomalies around the late seventies. This is the signature of the Great Salinity Anomaly (hereinafter GSA).

The GSA is the most important anomalous climatic variability in the North Atlantic related to sea ice. This feature was a widespread freshening of the upper layer of the subpolar gyre waters during 1968–1982 (Dickson et al., 1988). Some consider this episode as part of a pentadecadal oscillation, associated with fluctuations in the strength of the East Greenland current (Delworth, 1997), whereas for others (Mysak et al., 1990) it is one, exceptionally strong example, of a number of salinity anomalies that take place with a preferred decadal timescale. Possible pathways to explain the influence of ENSO and of the NAO on it have been outlined in Mysak et al. (1990) and in Mysak and Venegas (1998), respectively.

The mode of variability in Figs. 2 and 3a is undoubtedly relevant to the predictability due to the amount of variance explained, so we will use the time coefficient in Fig. 3a as an index to distinguish, among all the forecast months, those with more SIC (hereinafter ICE+), with a negative value of the time coefficient, from these with less SIC in the Greenland Sea (hereinafter ICE−), with a positive value of the coefficient.

The first EOF of the SST anomalies (explaining roughly 20% of the field variance, not shown)

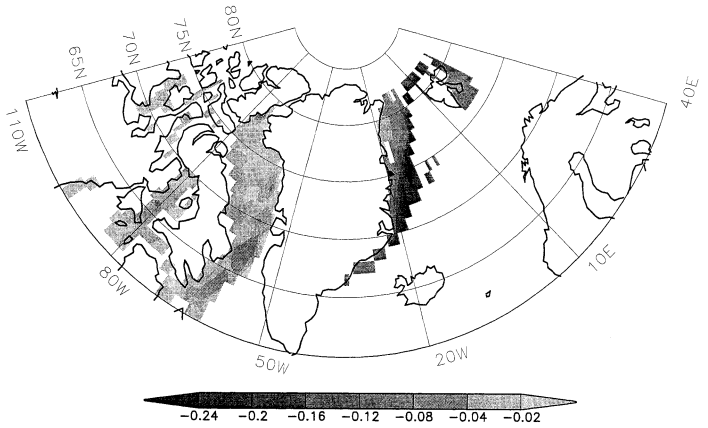

Fig. 2. First EOF of SIC anomalies during 1950–1998. The EOF accounts for a 66% of the total variance of the field.

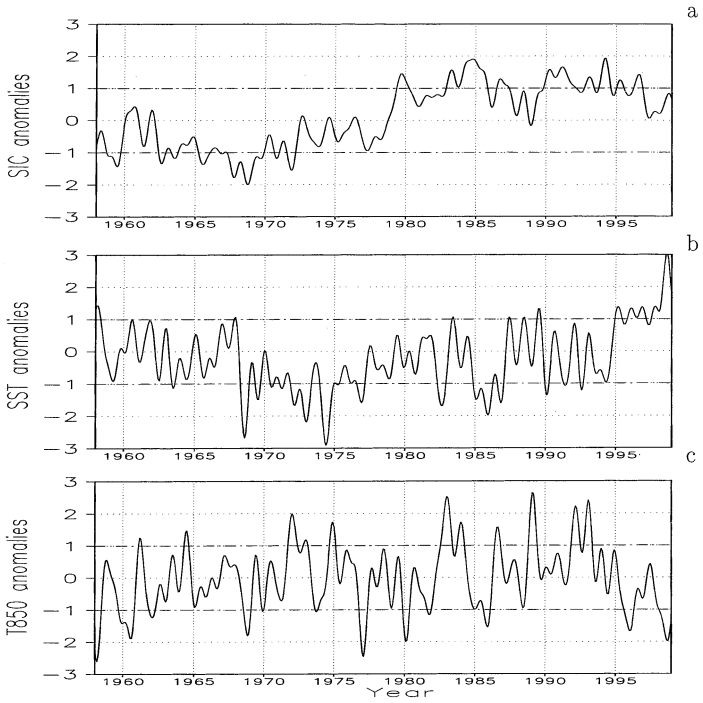

Fig. 3. Standardized time coefficients for the first EOF of the SIC anomalies (a), SST anomalies (b) and 850 hPa air temperature anomalies (c). The EOFs account for a 66%, 20% and 24% of the variance of each field, respectively. The time coefficients have been filtered to remove the variability with periods shorter than 8 months.

presents a center of anomalies near Newfoundland, with weaker anomalies of opposite signs to the north-east and south-west. The associated time coefficient in Fig. 3b shows the GSA signature from 1968 to 1982. The first EOF of the air temperature (explaining 24% of the variance of the field) presents a warm latitudinal band as response to the high-pressure centre in the Azores. The GSA period cannot be easily spotted from its temporal coefficient (Fig. 3c), which instead shows a high correlation (0.69) with the NAO index. The first EOF (50% of the variance) of the SLP field closely resembles the NAO pattern, with the two pressure cells centered around Iceland and the Azores. The GSA signature is again not that evident, while the correlation with the NAO index (0.82) is even higher than in the T850 case.

4. Forecast method and layout

For a forecast at a given lead l, we use the singular value decomposition (SVD) of the lagged cross-covariance matrix between predictor and predictand field. The SVD yields pairs of autovectors that correspond to coupled features where the time evolution of the predictor field must theoretically precede the time evolution of the predictand field at the lead time considered. Furthermore, the patterns can be ordered decreasingly by their corresponding singular value, which gives us the amount of the coupled covariance explained at lag l. A reduction of the number of degrees of freedom is then straightforward. Through the projection of each field onto the corresponding vector we obtain empirical coefficients of the time evolution of each pattern. In our predictive scheme, the predictor's evolution in time is related with that of the predictand through some empirical coefficients at lag l. Further details of the statistical method are given in Bretherton et al. (1992), Navarra (1993) and of the forecast scheme in SánchezGómez et al. (2001).

The scheme is summarized as follows: (1) the temporal filtering is applied to predictor and

predictand fields (Section 3); (2) the cross-covariance matrix is computed and the SVD calculations are carried out; (3) we obtain the time coefficients by the projection of each field onto the singular patterns; (4) a second filtering is performed by the reduction of degrees of freedom; (5) finally the forecasts are issued and its quality evaluated. In Fig. 4 we present schematically the procedure followed.

As already explained, the fields involved in this analysis are divided in two segments: training sample and validation period. The training sample includes those months used for the estimation of the parameters of the model. The validation period is the time interval to be forecasted. The procedure followed has been shown to produce a real forecast, not a hindcast, since only the 'past' is employed to issue a prediction. Almost four decades have been forecast in the case of SST (1960–1999) and the SLP (1960–1994) and nearly three (1970–1998) for the T850.

The optimal size of the training sample was investigated in SánchezGómez et al. (2001). The authors concluded that for fields originating from non-linear dynamics, relatively short training intervals (the tangent approximation) could perform better than longer datasets. In this work, the training interval is 120 months for the SLP and SST fields and 144 months for the air temperature field. It should be noted that the training sample is continuously updated, as SVD calculations are repeated whenever a month within the validation period is to be forecast.

As in many other recent forecast studies, the choice of the optimal number of patterns used in reconstruction and forecasts of the predictand field is partly based on the percentage of variance explained. We have also taken into account how well the NAO is represented in the filtered field. In Fig. 5 we present the percentage of variance explained by the predictand field as a function of the number of singular vectors retained. We also show there the correlation between the NAO index, as computed from the unfiltered predictand field, and the NAO index obtained from the filtered predictand field, against the number of singular vectors used in its reconstruction. Figure 5 suggests that a truncation after the fifteenth term would be satisfactory. Then, in all our forecasts, we have truncated the expansion after the fifteenth term for both the forecast field and the reconstructed predictand field.

The skill of the forecasts is assessed through the correlation between the predictand field (reconstructed with 15 patterns) and the forecast one. Values of the skill must be above the zero confidence interval, which can be roughly estimated at the 95% significance level as $S_s = 2/\sqrt{M}$, for values of M, the size of the validation period, greater than 20. We will call this value S_s the significant skill. Also, and because the number of spatial patterns used to forecast is not small, the problem

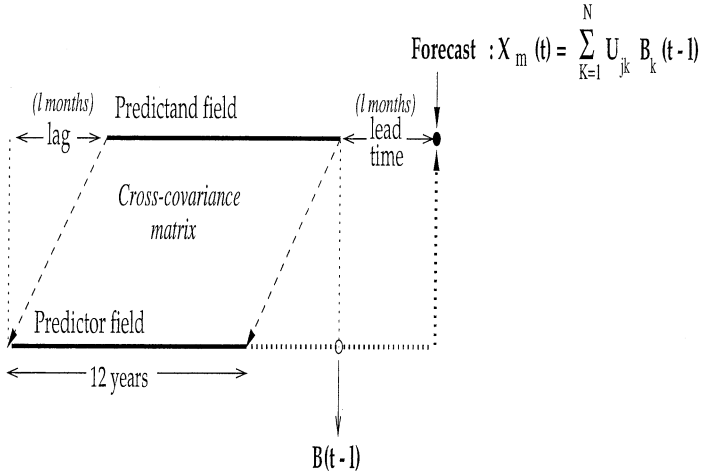

Fig. 4. Schematic representation of the forecast procedure. In all the experiments the lag between predictor and predictand coincides with the forecast lead time.

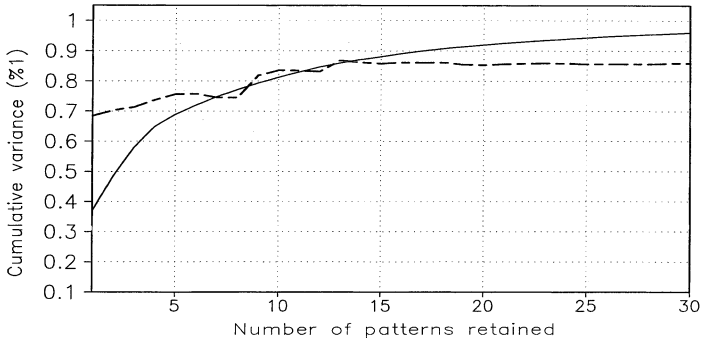

Fig. 5. Cumulative variance explained for the 850 air temperature anomalies (predictand field) as a function of the number of singular vectors retained (solid line). Correlation between the NAO indices respectively computed from the original field and from its reconstruction with the number of singular vectors on the horizontal axis (dashed line). The NAO index is computed as the difference between the 850 hPa air temperature anomalies averaged over the regions (25°W–2.5°W, 37.5°N–45°N) and (25°W–12.5°W, 62.5°N–70°N).

of an artificial skill obtained by overfitting has to be considered. This artificial skill, S_a, has been estimated from a large number (NE = 100) of Montecarlo forecast experiments following the same scheme presented above. For each of these, a different synthetic predictor field has been used. These field are a 'proxy' for the SIC anomalies, assuming that the evolution in time of this variable can be modelled by a Langevin equation (Lemke et al., 1980):

$$\frac{dy_t}{dt} = -\beta y_t + w_t \qquad (2)$$

where the feedback parameter β at each grid point (estimated from the observations) is fixed but w_t, the (white) driving noise, which represents the atmospheric forcing, has a different realization for each experiment. The average skill of those experiments provides an estimation of the artificial skill S_a.

As a control measure of the results given by the empirical model, the skill of the forecasts made by assuming persistence is also considered.

5. Forecast experiments and skill

5.1. Forecasts experiments and results

With the SIC anomalies as predictor, three main experiments are always carried out, corresponding to the three distinct predictand fields: North Atlantic SST anomalies, North Atlantic T850 anomalies and North Atlantic SLP anomalies. The respective validation periods are 1960–1998, 1970–1998 and 1960–1994.

Forecasts were produced at different lead times, ranging from 3 to 18 months, the skill of our model beats persistence for those greater than 6 months. Results are presented solely for the 12-month lead time, as values within the interval 8–15 months yield equivalent forecast skills.

Concerning the first experiment (SST is the predictand field), the highest skill occurs in the Gulf Stream region, near the coast of the Iberian Peninsula and in the Greenland, Iceland and Norwegian (hereinafter GIN) Seas. As shown in Fig. 6a, most of the skill in these northern regions (not shaded) seem to be due to persistence. For forecasts issued more than 12 months ahead, the forecast skill beats the persistence one (with values between 0.6 and 0.5) in the storm formation region near the Gulf of Mexico, and around the north-western part of the Iberian Peninsula.

As in the second experiment, prediction of the North Atlantic T850 anomalies, shown in Fig. 6b, the highest values of the skill seem to radiate from the tropics, thereby pointing to a tropical source for the skill. Skill levels (0.8 in the tropics) are higher than in the previous experiment. The forecast skill improves compared to persistence in the western part of the United States, the Caribbean Sea, the Canarian Archipelago and between Spain, France and the British Isles.

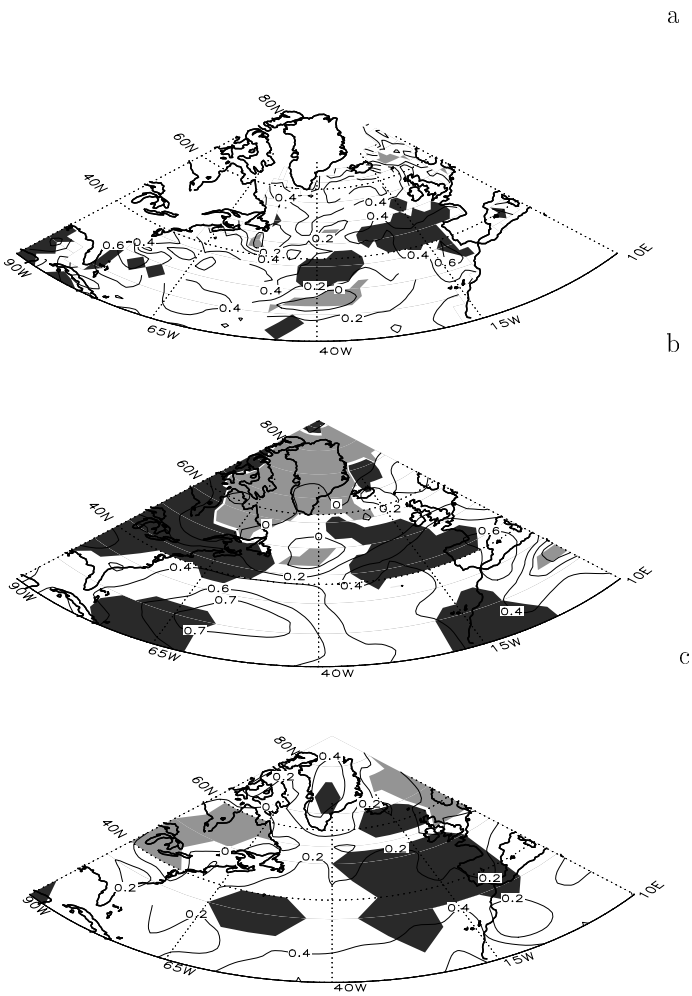

Fig. 6. Forecast skill for the whole period of validation for each of the experiments: (a) SST anomalies, (b) 850 hPa air temperature anomalies, and (c) SLP anomalies. The regions where the skill is under the values estimated for the artificial skill are indicated (light shaded). The regions where the skill of the model is above persistence are also emphasized (dark shaded). Contours above 0.6 have been represented by a thick line.

Results for the last experiment (prediction of North Atlantic SLP anomalies), as depicted in Fig. 6c, present values of the skill lower than those found in the other experiments. In some regions (Greenland, central North Atlantic and Africa) the skill for lead times from 3 to 6 months is above 0.5, but this value quickly drops to 0.3 for forecasts issued more than 5 months ahead. Only in a small region over Greenland do skill levels exceed 0.5 for lead times up to 15 months.

5.2. *Analysis of the origin of the forecast skill*

Additional analyses were carried out to identify the origin of the forecast skill. The goal is to try to establish the possible connection between the predictability in the North Atlantic region and the three relevant climate signals: the GSA, the ENSO and the NAO. Emphasis is put on the forecasts of air temperature anomalies 12 months ahead due to their greater success.

A decadal dependence of the skill can be readily seen if the forecast skill is determined separately for the seventies (Fig. 7a), eighties (Fig. 7b) and nineties (Fig. 7c). The loss of skill in the eighties is evident.

The seasonal dependence of the skill was also investigated in further detail. The observed and forecast fields have been separated according to the annual cycle: December, January and February for winter, and so on. Next the skill is computed for each of the seasons separately. The skill patterns obtained (not shown) indicate that the annual changes in the forecasts are slight (this is due presumably to the filtering), although more skillful predictions are scored preferably in winter and summer.

The first influence we address is that of GSA, a feature of the predictor that will be monitored by the first PC of this field (Fig. 3a). Negative values of this time series imply higher SIC around

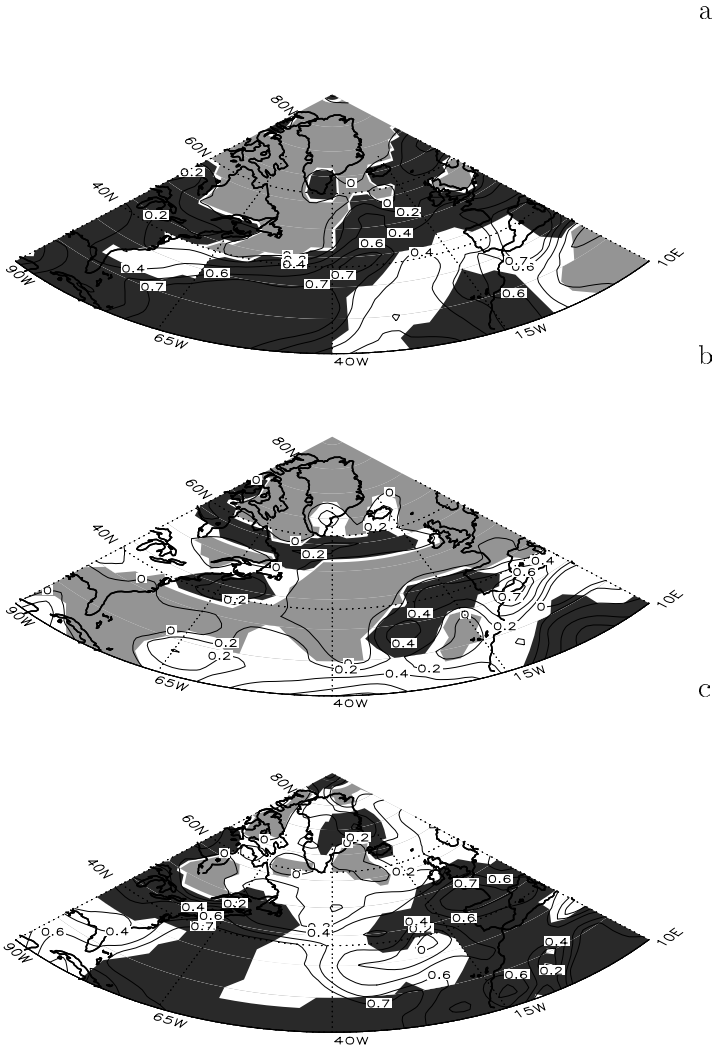

Fig. 7. Decadal dependence of the skill. Forecast skill for the seventies (a), eighties (b) and nineties (c) for the 850 hPa air temperature anomalies as predictand is represented. The regions where the skill is under the values estimated for the artificial skill are indicated (light shaded). The regions where the skill of the model is above persistence are also emphasized (dark shaded). Contours above 0.6 have been represented by a thick line.

Greenland (conditions refered as ICE+) whereas the opposite is true for positive values (ICE−). Forecast skill is computed separately for months under the distinct ICE+/ICE− conditions, in order to assess the effect of GSA on the predictability of air temperature. As the forecast period starts in 1970, the size of the ICE+ sample is much smaller than that of the ICE−. To avoid the statistical complexities that this would introduce, an ICE− sample of the same size as the ICE+ sample has been built, by including only the last months in the ICE− period. Figure 8 shows this dependence. It is clear from the figure that, in the ICE− case (Fig. 8b), the forecasts slightly improve in the north of the domain and worsen in a small region over the Iberian Peninsula and west coast of Africa in relation to the ICE+ case. In general, except for the regions mentioned, both ICE+ and ICE− conditions yield almost equivalent skill patterns. The fact that the forecast changes in the north and northeastern part of the domain suggests a local effect. The ICE− conditions seem to be more effective than the ICE+ in the exchanges with the overlying atmosphere. The regression pattern (not shown) of surface turbulent heat flux anomalies on the time coefficient of the first EOF of sea ice confirms this hypothesis (Deser et al., 2000). There is an above normal heat transfer from the ocean surface to the atmosphere when the first PC of sea ice (Fig. 3a) is positive. Additional composite analysis has been made (not shown) and indicates that the T850 anomalies during the ICE− conditions presents, with respect to the ICE+ situation, a significant warming over the east of Greenland, Europe and the rest of the domain south of 45° and a cooling west of Greenland and in the Baffin Bay. This goes along with the changes in intensity of the high- and low-pressure centers characteristic of the North Atlantic circulation.

The period of ICE+ goes from the beginning of the record to the late seventies. From that point onwards, conditions changed to the ICE− situation. Model forecasts for the eighties, trained

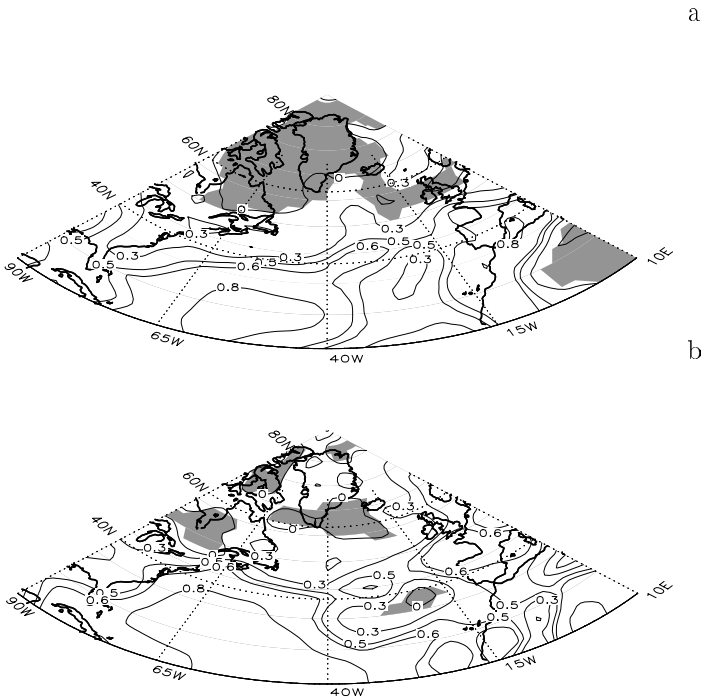

Fig. 8. Forecast skill corresponding to the 850 hPa air temperature for the ICE+ (a) and ICE− (b) conditions. The skill has been calculated as the correlation between the forecast and observed field through the period described in the text. The regions where the values of the skill are under those of the artificial skill are indicated by a light shading. Contours above 0.6 have been represented by a thick line.

under ICE+ air sea interactions, are unable to predict the ICE− situations, hence the drop of skill in this decade.

We have also investigated the extent to which such a remote signal as ENSO could affect the forecasts. Composites of the predictor (SIC) and predictand (T850) fields according to the phases of ENSO are presented in Fig. 9. The differences between the warm and cold phase are computed and tested for statistical significance using a univariate ANOVA test. From Fig. 9a it appears that during the warm (cold) events the SIC present negative (positive) anomalies in the Greenland Sea, and positive (negative) anomalies in the Labrador region. These changes, which might be ENSO induced over the T850 anomalies (Fig. 9b), are found significant in the subtropics, the Mediterranean region and in a small area over Baffin Bay and the Davis Strait. Note that in this study part of North and South Tropical Atlantic has been included. The picture shown in this figure is congruent with the influence of ENSO events on the Tropical Atlantic as stated by Lau (1997) and Klein et al. (1999). The mentioned works highlight how anomalies in the atmospheric circulation in the equatorial Pacific can produce changes in the evaporation and cloud cover, which in turn modify the heat flux flowing into the other remote tropical oceans. Concerning the North Tropical Atlantic, the warm events lead to a weakening of the trade winds, and consequently to a reduction in heat flux and a warming in its north-central part. These changes in the trade winds can be related to a weakening of the low-

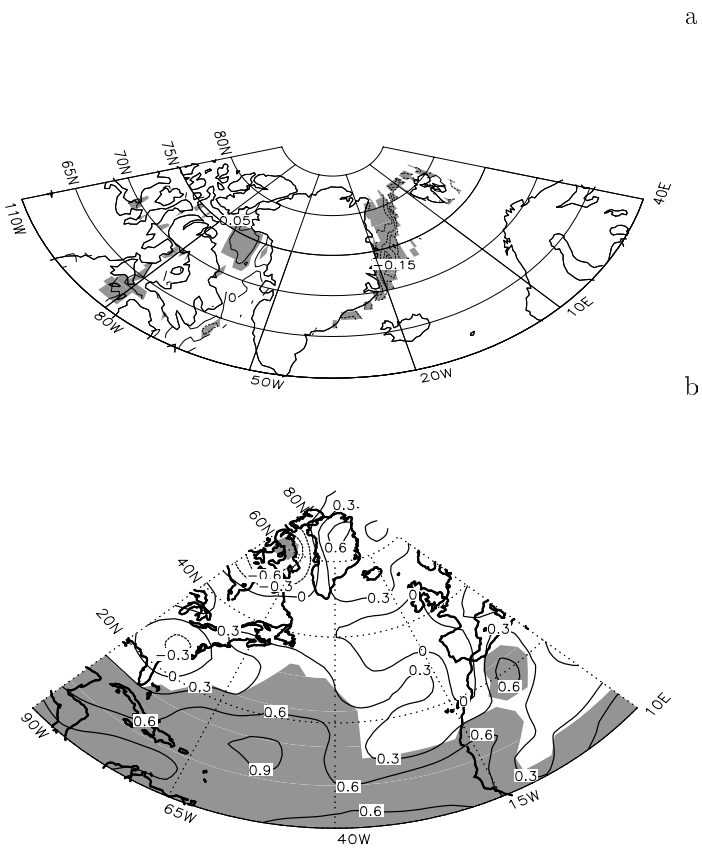

Fig. 9. (a) Composite analysis for the SIC anomalies according the ENSO phases. Differences between the warm and cold phase are computed and tested for statistical significance by an univariate ANOVA test. The shaded regions indicated where the difference is significant at 95% level. (b) Composite analysis for the T850 anomalies as in (a).

pressure center situated over the southeast United States (Klein et al., 1999), connected to the Pacific North American pattern (Wallace and Gutzler, 1981).

As ENSO influences both predictor and predictand fields, it seems reasonable to assess the changes that the warm (cold) phase of ENSO could induce on the forecasts. To compute an ENSO + skill we have taken into account the forecasts issued at months where the predictor field was already under the influence of a warm event. We have likewise proceeded to produce an ENSO − skill; in order to average to the same number of forecasts in both cases, the ENSO + events in the nineties have been excluded. The pattern of the ENSO + and ENSO − skill shows similar characteristics in the subtropics, where the higher values are found. To highlight the differences we have built an averaged skill over four regions where the differences between the ENSO + and the ENSO − cases are most important. These are the Labrador sea region (65°W–55°W, 45°N–55°N), an Iberian region (10°W–10°E, 35°N–45°N), the south Greenland region (50°W-30°W, 60°N–70°N) and the Great Lakes region (90°W–80°W, 35°N–50°N). In Fig. 10a we have represented the ENSO + skill at different leads for those regions, and in Fig. 10b we show the ENSO − case. We focus on the behaviour for lead times above 9 months. The improvement of the skill of forecast under ENSO + influence compared with the skill for ENSO − conditions is more significant in the Labrador and south Greenland region, and moderate in the Iberian region. In the case of the Great Lakes region, forecasts issued under ENSO − conditions are more succesful.

Lastly, we have also separated the forecast according to the NAO phase as determined by the sign of the NAO index. The skill for the NAO + and the NAO − phases are very similar and for this reason not shown. High values of the skill are confined to the region to the east of Bermuda and to the west Mediterranean.

6. Summary and conclusions

We have presented here the results of some empirical forecasts of anomalies in the North Atlantic basin. Three predictand fields are used: SST, T850 and SLP anomalies. The predictor field

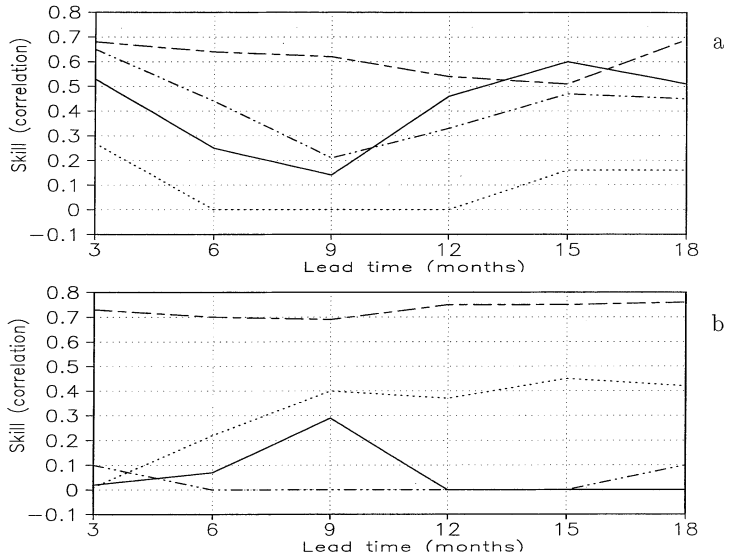

Fig. 10. (a) Dependence of the skill for the forecasts issued during ENSO + conditions on the forecast lead. The skill has been averaged over the four regions explained in the text: solid line for the Labrador region, long short dash for the Iberian region, dot dot dash for south of Greenland and dots for the Great Lakes. Horizontal axis is labelled in months. (b) As in (a) but for ENSO − conditions.

is the SIC anomalies over the GIN Seas, the Labrador Sea and the Davis Strait regions. The statistical technique used is based on the SVD of the lagged cross-covariance matrix between predictor and predictand fields. The lag is equal to the forecast lead. This technique has already been used in a previous paper by SánchezGómez et al. (2001). In that paper, T850 anomalies in the same domain (the North Atlantic) were forecast using SST anomalies as predictor field. The novelty of the present work lies mainly in the choice of the predictor field, the SIC anomalies, from the HadISST record. This predictor field allows us to focus on longer timescales of variability. It could be questionable, though, whether such a spatially confined predictor field can be an adequate predictor for a large-scale region such as the North Atlantic. The experiments discussed here have shown that the predictability of the SLP and SST is reduced to the region of sea ice interaction. However, the sea ice is a succesful predictor of the subtropical air temperature anomalies.

As for the record length, the use of reanalyzed data for both predictor and predictand fields allows forecasts to be issued for at least three decades. The forecasts have been formulated under a variety of climatic situations.

Preliminary spectral analysis shows important discrepancies in the high-frequency variability (timescales below 8 months) of the SIC and the atmospheric (air temperature) field. Because we are interested in forecasts at lead times around one year, and are aware of the risks of missfitting by introducing uncoupled signals in one field, the variability associated with timescales shorter than 8 months has been removed from predictor and predictand by filtering. This means that when comparing with other empirical seasonal forecasts performed on anomalies of seasonal mean values, the level of skill of our forecasts needs to be rescaled. This can be done by applying a correction factor, roughly estimated as 0.85, that is the averaged ratio of the filtered to the original variance.

Further analysis performed on predictor and predictand datasets points to a possible source of important discrepancy between the oceanic and atmospheric fields. In the oceanic fields, the period of the GSA stands out clearly, while this discrepancy is not as easily detected in the others. This fact will be of some relevance for the forecasts.

In the case of the SST forecasts, the skill is reasonably high in the adjacent regions to the sea ice, as in the GIN Seas. There is also some acceptable forecast skill in the eastern part of the subtropical gyre. The highest levels of skill appear in the T850 forecasts. This was also the variable best predicted with the SST anomalies in SánchezGómez et al. (2001). The source of this forecast skill seems to be the large-scale teleconnection pattern in Fig. 11, which represents the 12 months lagged correlation between the T850 anomalies and the first PC of sea ice (Fig. 3a). This pattern shows those regions where the predictor is most related to the predictand field, and therefore where the forecast is likely to be more succesful. Notice the resemblance with the pattern

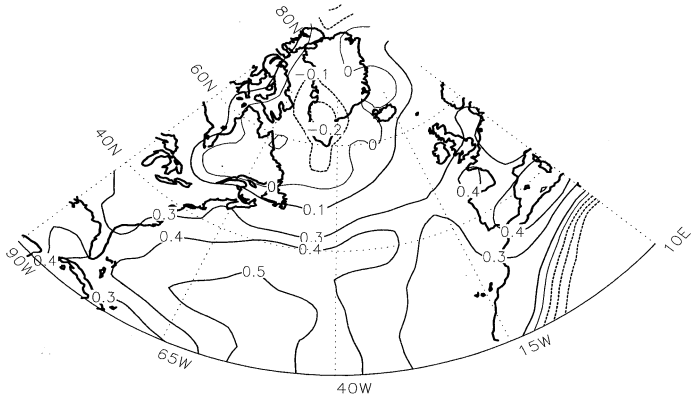

Fig. 11. Twelve-month lagged correlation between the T850 anomalies and the first PC of sea ice (leading). Values of correlation above 0.3 are found to be significant at the 0.95% confidence level according to a *t*-test.

of the skill shown in Fig. 6b. Inspection of Fig. 11 shows positive (negative) anomalies in the subtropical Atlantic, especially in the region centered east of Bermuda, and over the Iberian Peninsula and the Mediterranean region as well as negative (positive) anomalies over northeastern Canada and Greenland when the sea ice PC is positive (negative). Note that the pattern in Fig. 11 also presents a high resemblance to that associated with the NAO (Deser et al., 2000; Thompson et al., 2000). The warming over the eastern Greenland is related to reduced SIC over that region, and the cooling over the Labrador/Davis Strait is related to the increase of SIC.

Concerning the skill of the forecasts of SLP anomalies, only over Greenland does it attain values above 0.5, for leads up to 15 months. Therefore, it is inferred that the predictive skill from this empirical model at forecasting atmospheric anomalies, using SIC anomalies as predictor field, lies mainly in an ability to capture the thermodynamical part of the air–sea ice interactions.

Composites analysis shows that the warm (cold) phase of ENSO modifies the predictor field (T850) by producing a decrease (increase) of SIC in the GIN Sea and increase (decrease) of SIC over the Labrador Sea. The warmings or coolings in the subtropical Atlantic are the strongest part of the air temperature response to ENSO. During the warm phase of ENSO, and at the lead times of interest, the skill substantially improves in the Labrador and South Greenland regions, and to a lesser extent around Iberia. On the other hand, the forecasts issued for the Great Lakes under ENSO − conditions are considerably more skillfull than under ENSO + .

The structure of the skill for the two phases of the NAO resembles the pattern of the skill for the whole period of forecast, confirming that the NAO is the dominant mode of variability in the North Atlantic basin. However, the forecast skill appears to be relatively independent with respect to the phase of the NAO, in contrast to the results for the GSA and ENSO. This can be partially explained by the purely atmospheric and dynamical nature of the NAO. However, the lack of skill in the forecasts of the eighties would also explain it. Unfortunately, due to its decadal timescale, we have to take into account the three forecast decades to estimate NAO influence.

The analyses have shown the existence of a decadal dependence of the skill. This can be related to the fact that the training sample used to forecast the eighties was conditioned by a situation (the GSA) that was absent in the forecast period. The change from one state to the other is statistically unpredictable, even if we accept the recurrence of the Salinity Anomalies episodes. The duration of the GSA event imposes requirements in terms of training sample length that are unattainable with the available observations.

In the previous work by SánchezGómez et al. (2001), T850 anomalies were forecast using North Atlantic SST anomalies as predictor and the same forecast scheme. The same subtropical structure was responsible there for the highest levels of skill in both studies. Nevertheless, the use of SIC anomalies as predictor has enlarged the region where the forecasts beat persistence, compared with the forecasts issued with SST. The decadal dependence of the skill (also evident in the referred work), can be easily connected in this study with the GSA and the great differences in the air–sea interaction between the GSA period and the last part of the records.

7. Acknowledgements

Thanks are due to F. Alvarez for editing this manuscript and for his comments. We acknowledge here the Hadley Centre for Climate Research and Prediction (and particularly Nick Rayner) for both the GMSLP and HadISST1 datasets. This work was supported by the European Union under contract CT98-0714.

REFERENCES

Barnett T. P., Heinz, H. D. and Hasselmann, K. 1984. Statistical prediction of seasonal air temperature over Eurasia. *Tellus* **36A**, 132–146.

Bretherton C. S., Smith, C. and Wallace, J. M. 1992. An intercomparison of methods for finding coupled patterns in climate data. *J. Climate* **5**, 541–560.

Chapman W. E. and Walsh, J. E. 1993. Recent variation of sea ice and air temperature in high latitudes. *Bull. Am. Meteorol. Soc.* **74**, 33–47.

Curry R. E., McCartney, M. S. and Joyce, T. M. 1998. Oceanic transport of subpolar climate signals to mid-depths subtropical waters, *Nature* **391**, 575–577.

Delworth T. L., Manabe, S. and Stouffer, R. J. 1997. Multidecadal climate variations in the Greenland Sea and surrounding regions: a coupled model simulation. *Geophys. Res. Lett.* **24**, 257–260.

Deser C. and Blackmon, M. L. 1993. Surface climate variations over the North Atlantic Ocean during winter: 1900–1989. *J. Climate* **6**, 1743–1753.

Deser C., Walsh, J. E. and Timlin, M. S. 2000. Arctic sea ice variability in the context of recent atmospheric trends. *J. Climate* **13**, 617–633.

Dickson R. R., Meincke, J., Malmberg, S. A. and Lee, A. J. 1988. The 'Great Salinity Anomaly' in the northern North Atlantic 1968–1982. *Progr. Oceanogr.* **20**, 103–151.

Fang Z. and Wallace, J. M. 1994. Arctic sea ice variability on a timescale of weeks: its relation to atmospheric forcing. *J. Climate* **7**, 1897–1913.

Frankignoul C. and Hasselmann, K. 1977. Stochastic climate models. Part 2. Application to sea surface temperature anomalies and thermocline variability. *Tellus* **29**, 289–305.

Gloersen P. 1995. Modulation of hemispheric sea-ice cover by ENSO events. *Nature* **373**, 503–506.

Hurrell J. W. 1996. Influence of variations in extratropical wintertime teleconnections on the temperature variability of the Northern Hemisphere 500 hPa field. *Geophys. Res. Lett.* **33**, 665–668.

Johansson A., Barnston, A., Saha, A. and van der Dool, H. 1998. On the level and origin of seasonal variability forecast skill in Northern Europe. *J. Atmos. Sci.* **55**, 103–127.

Kalnay, E., et al. 1996. The NCEP/NCAR 40-year reanalysis project. *Bull. Am. Meteorol. Soc.* **77**, 437–471.

Klein S. A., Soden, B. J. and Lau, N. C. 1999. Remote sea surface temperature variations during ENSO: evidence for a tropical atmospheric bridge. *J. Climate* **12**, 917–932.

Lau N. C. 1997. Interactions between global SST anomalies and the midlatitude atmospheric circulation. *Bull. Am. Meteorol. Soc.* **122**, 21–33.

Lemke, P., Trinkl, E. W. and Hasselmann, K. 1980. Stochastic dynamic analysis of sea ice variability. *J. Phys. Oceanogr.* **10**, 2100–2120.

Mysak, L. A., Manak, D. K. and Marsden, R. F. 1990. Sea ice anomalies observed in the Greenland and Labrador Seas during 1901–1984 and their relationship to an interdecadal Arctic climate cycle. *Clim. Dynam.* **5**, 111–133.

Mysak L. A. and Venegas, S. 1998. Decadal climate oscillations in the Arctic: a new feedback loop for atmosphere–ice–ocean interactions. *Geophys. Res. Lett.* **25**, 3607–3610.

Mysak, L. A., Ingram, R. G., Wang, J. and van der Baaren, A. 1996. The anomalous sea-ice extent in the Hudson Bay, Baffin Bay and Labrador Sea during three simultaneous NAO and ENSO episodes. *Atmos. Ocean* **34**, 313–343.

Navarra, A. 1993. A new set of orthonormal modes for linearized meteorological problems. *J. Atmos. Sci.* **50**, 2569–2583.

Palmer, T. N. and Sun, Z. B. 1985. A modeling and observational study of the relationship of sea surface temperature in the north-western Atlantic and the atmospheric general circulation. *Quart. J. R. Meteorol. Soc.* **111**, 947–925.

Pickart, R. S., Spall, M. A. and Lazier, J. R. N. 1997. Mid-depth ventilation in the western boundary current system of the subpolar gyre. *Deep-Sea Res. Part I* **44**, 1025–1037.

Radcliffe R. A. S. and Murray, R. 1970. New lag associations between North Atlantic sea temperature and European pressure applied to long-range weather forecasting. *Quart. J. R. Meteorol. Soc.* **96**, 236–246.

Rayner, N. A., Parker, D. E., Frich, P., Horton, E. B., Folland, C. K. and Alexander, L. V. 2000. SST and sea-ice fields for ERA-40. *Proceedings of the Second WCRP International Conference on Reanalysis, WCR 109 (WMO/TD-NO. 985)*, 18–22.

SanchezGómez, E., Álvarez, F. and OrtizBeviá, M. J. in press. Empirical prediction of 850 hPa North Atlantic air temperature anomalies. *Quart. J. R. Meteorol. Soc.*, accepted for publication.

Thompson, D. W. J. and Wallace, J. M. 1998. The Arctic oscillation signature in the wintertime geopotential height and temperature fields. *Geophys. Res. Lett.* **25**, 1297–1300.

Trenberth, K. E. 1996. The definition of El Niño. *Bull. Am. Meteorol. Soc.* **78**, 2771–2777.

Vautard, R., Plaut, G., Wang, R. and Brunet, G. 1998. Seasonal prediction of North America surface air temperature using space–time principal components. *J. Climate* **10**, 389–394.

Wallace, J. M. and Gutzler, D. S. 1981. Teleconnections in the geoptential height field during the Northern Hemisphere winter. *Mon. Wea. Rev.* **109**, 784–812.

Walsh, J. E. and Johnson, C.M. 1979. Interannual atmospheric variability and associated fluctuations in Arctic sea ice extent. *J. Geophys. Res.* **84**, 6915–6928.